Three-Dimensional Numerical Simulation of Induction Loggings

Carrasco, A. & Carrasquilla, A. ; LENEP – UENF; Macaé -RJ

Abstract

The electromagnetic induction well log method is one of the more utilized geophysical logs in oil industry, aiming to obtain petrophysical informations regarding geological formations along the well. Although there are some new and advanced induction tools, as Phasor and Array Induction Tool, in this work we used some classical SCHLUMBERGER tools, as 2C40, ILD and 6FF40, with the objective of testing new algorithms, which can show a better way to interpret complex geological media. With this aim, we use the integral equation numerical method, which has been applied successfully with other geophysical techniques. In our specific case, these results were compared to the response of models that were simulated with the numerical algorithm of finite differences and, subsequently, were applied in the evaluation of responses of three-dimensional heterogeneities in well common three-dimensional environments, as invasion front, fractures, etc.

Introduction

The electromagnetic well induction logging was developed in the late 40's in order to measure the electric conductivity (σ) of the layers in resistivity muds wells. Its inverse, the electric resistivity (ρ=1/σ), is one of the most important parameters used to measure the production potential of a well, either oil or gas. These parameters are used in order to avaluate some petrophysical properties as water saturation, invasion front and resistivity anisotropy in slant wells.

To understand the wellbore responses during the electric resistivity measurements, computer numerical simulations are generally used. These simulations, when made in one or bidimensional way, help to understand many situations, as drilling mud invasion or fall formations in the well, and , this kind of simulations must be done three-dimensionally (3D) to get a better approximation of the reality.

Simulations of geologic enviroments were made using the 3D scheme and some numerical techniques as finite element, finite differences, integral equation or hibrid methods (ANDERSON & BARBER, 1988). In this work, we used the integral equation method, which includes the primary field calculation (1D stratified layers) and the discretization in cells of the secondary field (3D body). This method were used for different induction arragements.

Methodogy

Geophysical logging plays an important role in petroleum exploration, mainly in the characterization petrophysiical characteristics of reservoirs, because of their low cost and the important information offered from the rock formations.

In our study we use the 2C40, 6FF40 and ILD (*Induction Log Deep*) arrangements, all of them from the SCHLUMBERGER company. Nowadays, there are in the industry anothers probes with better resolution and deeper investigation characteristics, as the Array Induction Tool or Phasor, but in this work the use of classical tools is justified as a way to test new algorithms, which can help in the interpretation of 3D geological enviroments.

The first step of our work was to develop the 1D forward algorithm, which constitutes the rest rock of the 3D heterogeneities. This kind of solution is based on the exact response of the Green problem, that is, the determination of the electromagnetic field inside a stratified medium. Thus, the source of a classical induction probe is composed by a magnetic dipole and the measure is along the well axis. If we work in a cilindrical coordinate system, the magnetic potential vector takes part of the Helmholtz equation as:

$$\nabla^2 \overline{F_z} + k^2 \overline{F_z} = 0 \qquad (1)$$

and the electric field is given by:

$$\overline{E} = -\nabla \times \overline{F} \,. \qquad (2)$$

Also, the components of the electric fields are:

$$E_r = 0, \quad E_Z = 0, \quad E_f = iwm \frac{\partial F_Z}{\partial r} \qquad (3).$$

Near the source, the potential vector F_z of the magnetic dipole is:

$$F_z = \frac{.m_z}{4p} \frac{e^{-ikR}}{R} \,. \qquad (4)$$

Finally, to solve the Equation (1), we will obtain the response in the following general form:

$$F_Z = \int_0^\infty [a_m e^{-b_m Z} + b_m e^{b_m Z}] l J_0(lr) dl \,. \qquad (5)$$

In this expression, a_m and b_m are constants, z is the vertical coordinate, l is the integration variable, b_m is the propagation constant and J_o is the *Bessel* function of first kind and zero order. The a_m e b_m values take different forms according with the relative positions of the transmissor and receptor for each layer considered.

To obtain the electromagnetical response of a 3D body, the integral equation scheme is used introducing the scattering current concept into the formulation. The electric field may be solved using the appropriate Green functions (HOHMANN, 1971).

The integral equation technique considers only the discretization of the non-homogeneus part, which permit to use less memory and reduces the computation time. For this reason, it is considered the best numerical method to solve 3D electromagnetic problems in the case of small and concentrated heterogeneities (CARRASQUILLA, 1993).

Considering a 3D body and the Maxwell Equations, using MKS units (e^{iwt} time dependent), these ca be expressed in the following form:

$$-\nabla\times\overline{E} = \hat{z}\overline{H} + M_i, \quad (6)$$

$$\nabla\times\overline{H} = \hat{y}\overline{E} + J_i, \quad (7)$$

where M_i and J_i are the magnetic and electric currents, and $\hat{z}$ and $\hat{y}$ are the impeditivity and admitivity. These expressions are given by $\hat{z} = iwm$ and $\hat{y} = s + iwe$, respectively.

HARRINGTON (1968) showed that using an integral equation, the electric field can be formulated as:

$$\nabla\times H = s_1 E + J_S + J_i, \quad (8)$$

where: Js is the scattering current of the body (Js = (s_2 – s_1)E). s_2 and s_1 are the heterogeneity conductivity and the conductivity of the medium, respectively.

Taking the rotational of Equation (7) and replacing $\tilde{N} \times H$, we obtain an heterogeneous vector:

$$\nabla\times\nabla\times E - k^2 E = -iwm_0(J_S + J_i) - \nabla\times M_i, \quad (9)$$

where $k^2 = w^2 m_0 e_0$ is the propagation constant. Also:

$$E = E_i + E_s, \quad (10)$$

where E_i and E_s represent the incident and scattering field respectively, which satisfies the following equations:

$$\nabla\times\nabla\times E_i - k^2 E_i = -iwm_0 J_i - \nabla\times M_i \quad (11)$$

$$\nabla\times\nabla\times E_S - k^2 E_S = -iwm_0 J_S. \quad (12)$$

The solution of the Equation (11) corresponds to the electric fields of the sources. On the other hand, to solve the Equation (12), we considered *Js* as an ordinary source. So, multiplying with the appropriated dyadic function and making an integration around the heterogeneity, we have:

$$E_S(r) = \int_V \hat{G}(r,r').J_S(r')dV', \quad (13)$$

where G(r,r') is the dyadic Green function of the electric field at *r* for an element current, having as reference another current point at *r'* , at the interface earth-air. G is expressed by VAN BLADEL (1961) apud (HOHMANN, 1975) as:

$$\hat{G}(r,r') = \frac{1}{s_1}[k_1^2 g - \nabla\nabla']G(r,r'), \quad (14)$$

where *g* is the dyadic identity and G is a Green scalar function. The expression for all the space is given by:

$$G(r,r') = \frac{e^{-ik_1 R}}{4pR}, \quad (15)$$

where $R = |r - r'|$ and $k_1 = (-iwm_o s_1)^{1/2}$. Replacing *Js* into the Equation (13), the expression results in:

$$E(r) = E_i(r) + (s_2 - s_1)\int_V \hat{G}(r,r').E(r')dV'. \quad (16)$$

This equation is known as the second order integral of Fredholm, singular and heterogeneous, with the electric field solved inside the body (HOHMANN, 1975). So, we approximate the integral equation setting the body as small cubic cells with ? of dimension. Then, we have a finite summation for every field in each sub cell at *n*:

$$E(r) = E_i(r) + (s_2 - s_1).\sum_{n=1}^{N}\int_{Vn}\hat{G}(r,r')dV'.E_n, \quad (17)$$

where:

- E(r) is the total electric field,
- $E_i(r)$ is the primary electric field of the surrounding medium, calculated for every SCHLUMBERGER probe,
- $\hat{G}(r,r')$ is the dyadic Green function which relates the electric field at *r* with a current element at *r'*,
- E_n is the total electric field discretized in *n* cubic cells,
- (s_2 – s_1) is the difference of conductivities between the heterogeneous body and the surrounding medium,
- dV is the differential function of the dyadic Green expression.

Equation (17) can be modified depending on the base function chosen to represent *?sE* (also named as J_S). The easiest form to do this, is dividing the body into N cells, using a base function (XIONG, 1999):

$$E(r) = E_i(r) + \frac{(s_2 - s_1)}{s_1}\sum_{n=1}^{N}\Gamma(r,r')\,E_n, \quad (18)$$

where G is the dyadic Green function for a cubic element of volume. From Equation (18) we can express the electric field for each cell as:

$$\sum_{n=1}^{N}\left[\frac{s_2 - s_1}{s_1}\Gamma_{mn} - d_{mn}\right]E_n = -E_m^{-1}, \quad (19)$$

where

$$d_{mn} = \begin{cases}\Theta, & m = n\\ 0, & m \neq n\end{cases}, \quad (20)$$

d_{mn} is the *Kronecker* delta, and T is the tensorial unit. This expression can be written as:

$$[\Gamma][J_S] = [E_n]. \quad (21)$$

Usually, the coefficient matrix G of Equation (21) is referred as scattering matrix (XIONG, 1999). To solve it, we considered each cell coupled using the Green function and composed by a primary and scattering component.

RESULTS AND INTERPRETATION

Firstly, in order to test our 1D program, we consider a group of models studied by ROJAS (1995) in his doctorate thesis. One of these models is composed by a sequence of 27 layers known as Oklahoma Formation (Unites States), which is used as a benchmark in the petroleum industry. Figure 1 shows the apparent resistivities calculated by the ILD, 2C40 and 6FF40 probes, besides the ROJAS (1995) results for the 6FF40 probe. Evaluating these responses, we found similarities among them. We also test our 1D algorithm with a model found in the master degree thesis of VIERA (1990), who used the ANDERSON & CHANG (1982) algorithm. He calculated the 2C40 response for a model composed by two layers of 0.2 Ω.m and 20 Ω.m of resistivity (Figure 2). In this figure, the straight lines represent the model, the curve line is the response of the algorithm and the circles on it represent the ANDERSON & CHANG (1982) results. In this case, it exists a perfect fitting between both results.

In relation to 3D results, we used two groups of models, the first one composed by 2.5 D models, already tested by ROJAS (1995), and the other one, related to particular cases refered to different kind of complex 3D geological environments. In his simulations, ROJAS (1995) used the finite difference method with axial symmetry (2.5D) in their models. First, we simulated a wellbore as a 3D body, with a resistivity of 1 ohm-m, placed into a sequence of three layers, as shown in the Figure 3. In this model, the well logging response corresponds to the 2C40 arrangement, obtaining similar results with the ROJAS (1995) (Figure 4). In this figure, the difference between the resistivity values affected by the drilling mud (1 ohm-m) and the values obtained from our algorithm (without considering the wellbore effect), are very small.

In the sequence, we tested a new model (Figure 5), considering the wellbore effect, in a resistivity sequence of 1-200-1 Ω.m, but now using the 6FF40 arrangement. In this sense, we note, again, a good agreement between the ROJAS (1995) response and the obtained in our work (Figure 6).

In the next step, we studied different complex 3D geological environments. Firstly, we simulated a fracture as WANG (2003) simulated, who evaluated the three components of the apparent conductivity using multicomponent induction, and realized that each component had different responses when a vertical fracture is present. The resistivity formation for this model is 1 Ω.m, mud drilling with 1000 Ω.m, wellbore diameter of 0.3048m (12 inches) and a fracture length of 0.0254 m (1 inch). So, the 3D body characteristics of this model are shown in the Figure 7 (not in a designed scale). For this case, the resistivity of the fracture is the same of the drilling mud (1000 Ω.m) with a fracture extension of 1.5 m.

The result for this model was an average resistivity of 8.24 Ω.m (Figure 8), value that corresponds approximately to the conductivity of 120 mS/m, depending on the extension of the fracture. According to WANG (2003), the response for this model is nearly 200 mS/m. This value reflects the effect of the high resistivity of the fracture (1000 Ω.m), in according with the values got by Wang (2003).

Another tested model deals with a situation when the wall of the wellbore is falling, making its diameter bigger than the adjacent sections. Here, we created a model with an intermediate layer of 1.5 m, 100 Ω.m of resistivity, and invasion drilling fluid of 0.5 m with 1 Ω.m of resistivity (Figure 9). The resulting log is shown in Figure 10. The differences at the intermediate layer are given by the inflexions present, because of the intrusion of the low resistivity mud (1 Ω.m). The 2C40 probe was used for this case.

Finally, we simulated the logs response from the 2C40, 6FF40 and ILD probes, using a model with different invasion radios. The resistivity distribution corresponds to an aquifer (Figure 11). So, the diameter of the wellbore is 0.2 with 120 Ω.m. Near to this section, the area numbered as 2 corresponds to the first invasion radio (0.6m), represented by a resistivity of 150 Ω.m. In its vicinity, we found the zone numbered as 3, which correspond to a transition zone, with 80 Ω.m of resistivity and 1.2 m of radio. All this section is positioned into a layer of 20 Ω.m which corresponds to a virgin zone.

The logs obtained from this three probes are shown in the Figure 12. Here, the 2C40 log resistivity values of the adjacent layers are greater than 1 Ω.m, because of the strong influence of the resistivity of the wellbore and the lower investigation potential of this tool. In the invasion zone, the highest value is 80 Ω.m, approximately. Moreover, the ILD response in this layer has a maximum value of 29 Ω.m, showing the possibility of being in the transition zone, but still with a strong influence of the adjacent layers. The apparent resistivity values of the adjacent zone are near to 1 Ω.m. Finally, the response of the 6FF40 probe shows a maximum value of 14 Ω.m, and this value would correspond to the virgin zone, but always with some influence of the adjacent layers. The values of the apparent resistivities in the adjacent layers are near to 1 Ω.m, as the ILD case.

With the same dimensions of the last model, we changed the resistivity distribution to simulate an oil reservoir. Those distribution resistivities were taken from the *Institute of Geophysics of Nobosibirsk State University, Rússia* (Institute of Geophysics, 2002), as shown in the Figure 13. The response of this model appears in the Figure 14, where the 2C40 log does not register any significant variation in the resistivities because of the low resistivity value of the drilling mud (2 Ω.m) and the strong influence of the adjacent layers (1 Ω.m).
The ILD log shows higher apparent resistivities (10 Ω.m), reaching probably the washed zone (20 Ω.m) and, as the former case, we observe a better performance of the 6FF40 tool, with slightly higher values but still influenced by the adjacent layers.

CONCLUSIONS

This work illustrates the performance of induction tools in geological enviroments considered as complex. The use classical arrangements as 2C40, ILD and 6FF40 from the SCHLUMBERGER company, helped to test new algorithms for three dimensional interpretation in complex enviroments.

On the first stage of this work, we succesfully tested the 1D algorithm. After that, we introduce this 1D algorithm as part of the method of the integral equations for 3D interpretations. This methodology showed a high degree of efficient responses. We also tested our results with previous models used with other algorithms.

In a second stage, we use our tested algorithm to modelate three dimensional geologic enviroments with particular characteristics, as in example: vertical fractures, wellbore with zones of falling walls, wellbore with different invasion diameters, etc. The quality of the responses obtained with these models, makes possible to model many other situations of complex geology. The speed of calculation of the program depends on the number of cells used, reaching 15 minutes when the number of cells is 420, in a computer with a total virtual memory of 894,180 kB, hard disk of 31.3GB, 996 M Hz, in LINUX environment. Using less number of cells (180), the execution time will be less than 15 seconds.

For future works, it is recommended to employ more advanced probes, as Phasor (SCHLUMBERGER), or the russian Vikiz. In this sense, it could be possible to make some changes in the primary field using the same scheme of numerical modelling, with the objetive of modelling slant or horizontal wells.

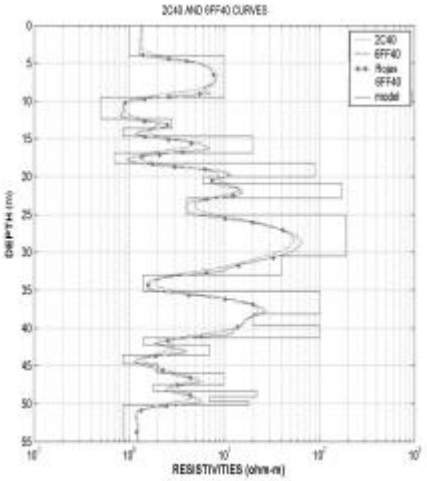

Figure 1. Sintetic Curves for 2C40 and 6FF40 probes

ACKNOWLEDMENTS

The authors would like to thank to LENEP/UENF for the computational support and to UENF and CNPq for the doutorate scholarship and productivity research, respectively.

REFERENCES

- Anderson, *B.* 1988. The analysis of some unsolved induction interpretation problems using computer modeling. *The Log Analyst*. 60-73.
- Carrasquilla, A. A. 1993. *Modelagem Numérica da influencia do eletrojato equatorial em dados magnetotelúricos produzidos por estruturas 3D,* Tese de Doutorado, Belém-Pará, 176 p.
- Chang, S. K. & Anderson, B. 1982. Simulation of induction logging by the finite-element method. *Geophysics*, 49, 1943-1958.
- Hohmann, G. W. 1975. Three-dimensional induced polarization and electromagnetic modeling. *Geophysics*. 309-324.
- Rojas, P. A. 1995*. The Forward and Inverse Problems in Induction Logging.* Doctorate these, Colorado School of Mines.
- Wang, T. 2003. Characterizing drilling-induced fractures with multicomponent induction and acoustic data. *Sociedade Brasileira de Geofísica*.

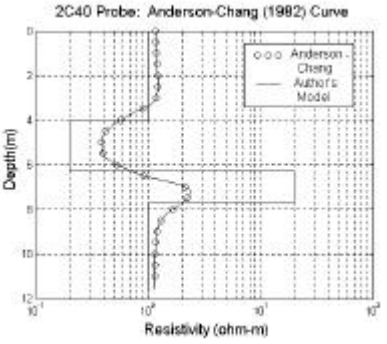

Figure 2. Comparison between 1D responses with 2C40 arrangement using our algorithm and that of the Anderson and Chang (1982)

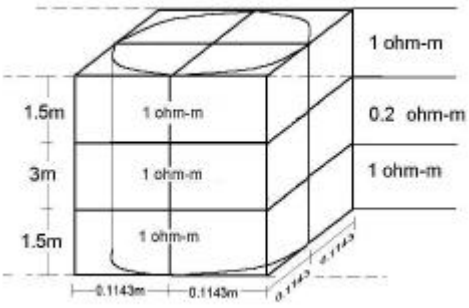

Figure. 3. Model 1: Intemediate layer with low resistivity

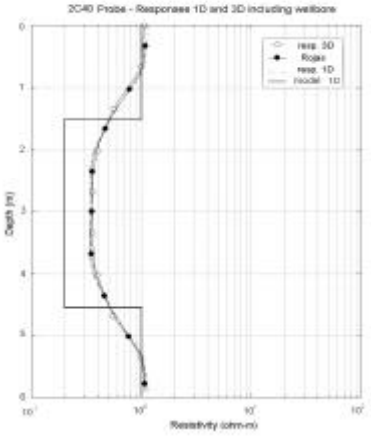

Figure 4. Response of Model 1 using 2C40 probe.

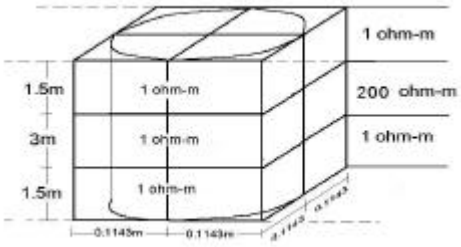

Figure 5. Model 2: Intermediate layer with high resistivity

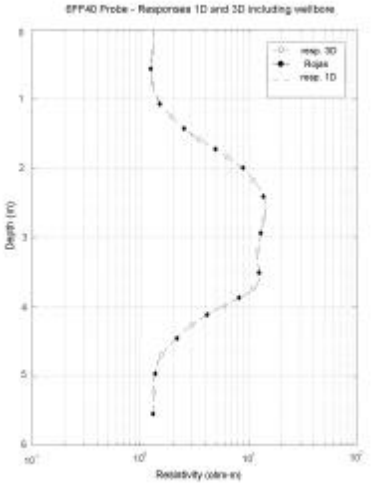

Figure 6. Response of Model 2 with 6FF40 probe

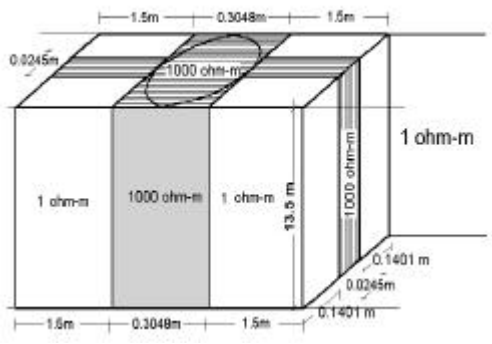

Figure 7. Model 3: 3D body simulating a fracture in an homogeneous medium.

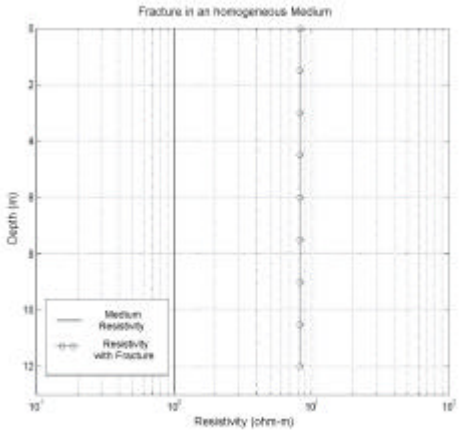

Figure 8. Fracture Response in a homogeneus medium

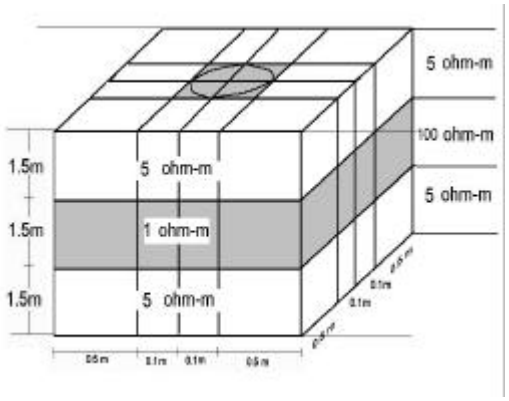

Figure 9. Model 4: Wall falling in an intermediate layer.

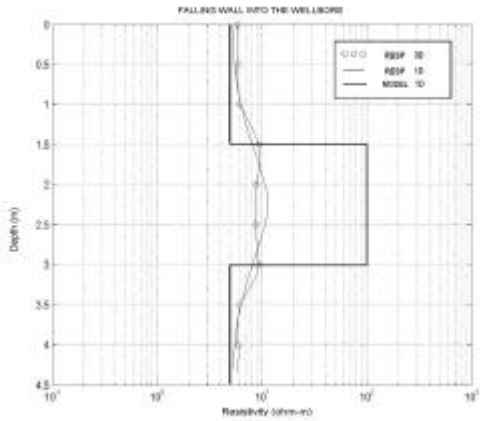

Figura 10. Response of Model 4 using 2C40.

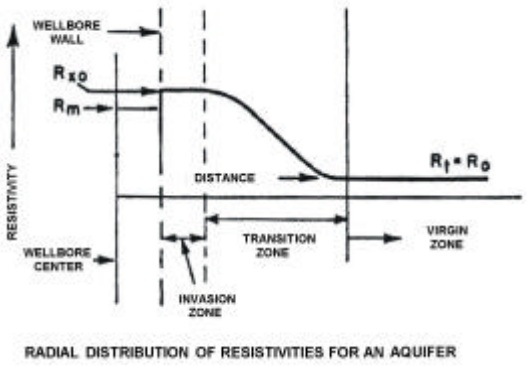

Figure 11. Radial Distribution of Resistivities for an aquifer (SCHLUMBERGER, 1972)

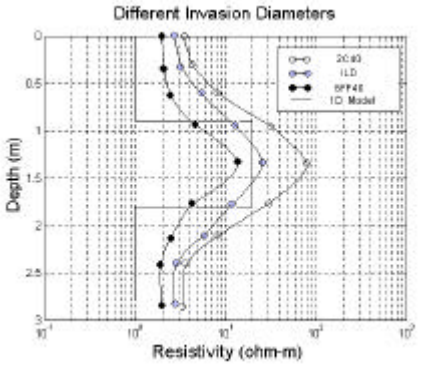

Figure 12. Response for the Y3 model

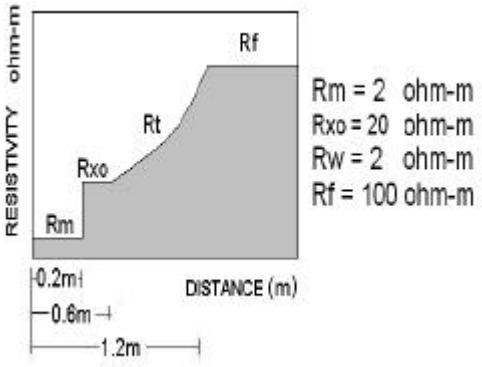

Figura 13. Model 6: Radial distribution of resistivities for an oil reservoir (adapted from the Institute of Ge o-physics, 2002).

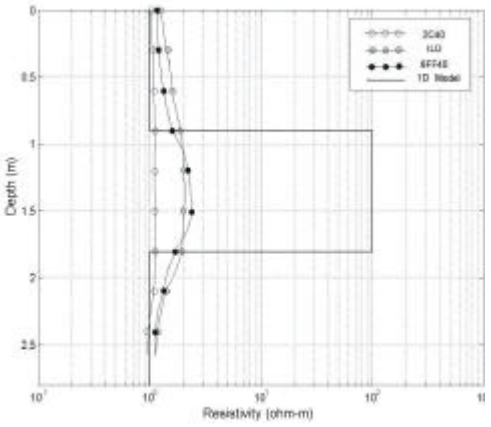

Figura 14. Response for Model 6.